Laser Machining of Ablating Materials – Overlapped Grooves and Entrance/Exit Effects

Michael F. Modest and Sriram Ramanathan
Department of Mechanical Engineering
The Pennsylvania State University
University Park, PA 16802
Ph: (814)863-0976 FAX: (814)863-8682

Armin Raiber and Birgit Angstenberger
Institut für Strahlwerkzeuge
University of Stuttgart
Pfaffenwaldring 43
70569 Stuttgart, GERMANY
Ph: (0711)685-6840, FAX: (0711)685-6842

Abstract

A three-dimensional conduction model has been developed to predict the transient temperature distribution inside a thick solid that is irradiated by a moving laser source, and the changing shape of single or overlapping grooves carved into it by evaporation of material. The laser may operate in CW or in pulsed mode (with arbitrary temporal intensity distribution) and may have an arbitrary spatial intensity profile. The governing equations are solved, for both constant and variable thermophysical properties, using a finite-difference method on a boundary-fitted coordinate system. Results are presented for ablative groove development, including the effects of laser entry and exit (laser scanning across the edge of the material), single and overlapped groove shapes and temperature distributions in the solid at different traverse speeds, pulsing conditions and power levels. Experimental results were obtained for groove shapes of single and overlapped grooves, using graphite as the ablating material and employing a CW CO_2 laser (10.6 μm) focused with a 5-inch lens for powers ranging from 400 to 1200 W and scanning speeds ranging from 2.5 to 10 cm/s. Comparison between experimental and theoretical results indicates good qualitative agreement between theory and experiment within the limits of the (rather large) uncertainty with which material properties are known to date.

INTRODUCTION

Since their invention in 1960, lasers have found diverse applications in engineering and industry because of their ability to produce high-power beams. Laser applications include welding, drilling, cutting, scribing, machining, heat treatment, medical surgery, and others.

One of the principle advantages of laser cutting is its ability to cut very hard materials easily. Ceramics are among the most difficult materials to machine by conventional machining techniques, since they are very hard and brittle. The cost of machining ceramics into complex shapes is often prohibitive if conventional machining is used. Lasers may provide a cheaper alternative to conventional machining and have found wide-spread use in industry. However, the physical phenomena involved in many laser applications are not fully understood. A better quantitative

understanding of the physical mechanisms governing these phenomena will diminish the need for extensive trial and error experiments, in orfder to employ lasers for complex machining operations on newly developed materials.

Modeling of laser drilling, cutting and scribing has been addressed by a number of investigators. Simple one-dimensional drilling models have been given by Dabby and Paek [1] and Wagner [2]. Other approximate laser drilling models have been developed by Schuöcker and Abel [3], Petring *et al.* [4], Chen and Mazumder [5], and others. Laser scribing, drilling and cutting of materials taking into account ablation and/or decomposition has been investigated primarily by Modest and coworkers. They developed a number of models [6–17], ranging from quasi-onedimensional to fully three-dimensional models. The reader is referred to these papers for a complete description of their various aims and capabilities, as well as to a monograph by Chryssolouris [18] for a review of other pertinent theoretical work that has dealt with the different aspects of material removal with lasers.

All theoretical models to date dealing with a scanning laser, with the exception of Modest [19], have dealt only with quasi-steady material removal using a CW (continuous wave) laser. In the present paper the transient three-dimensional finite-difference model on a boundary-fitted coordinate system of Modest [19] will be extended to allow the treatment of material entry and exit effects, as well as the analysis of multiple, parallel, partially-overlapping grooves.

THEORETICAL BACKGROUND

The underlying theory of the present paper is identical to Ref. [19] and is, therefore, subject to the same assumptions, which are repeated here for convenience:

1. The solid moves with constant velocity u.
2. The solid is isotropic.
3. The density variation with temperature in the solid is negligible.
4. The material is opaque, *i.e.*, the laser beam does not penetrate appreciably into the medium.
5. Change of phase from solid to vapor (or decomposition products) occurs in a single step with a rate governed by a simple Arrhenius relation. Real materials may display significantly different behavior as discussed by Roy and Modest [14]. Such effects are included by employing the total amount of energy required to remove material, referred to as "heat of removal", Δh_{re}.
6. The evaporated material does not interfere with the incoming laser beam and ionization of the gas does not occur, *i.e.*, the gas is transparent and there are no droplets and particles (or they are removed by an external gas jet).
7. Heat losses by convection and radiation (on top surface and sidewalls) are negligible as compared to the intensity of the incident beam (Modest and Abakians, [7]).
8. Multiple reflections of laser radiation within the groove are neglected, restricting the present model to shallow grooves or materials with high absorptivities. Multiple reflections of laser radiation within the groove have been addressed by Bang and Modest [16, 15, 17].

The transient heat transfer equation for a thick solid (with constant density ρ) of length L_{wp} and width W_{wp}, with a Cartesian coordinate system fixed to the solid, irradiated by a Gaussian

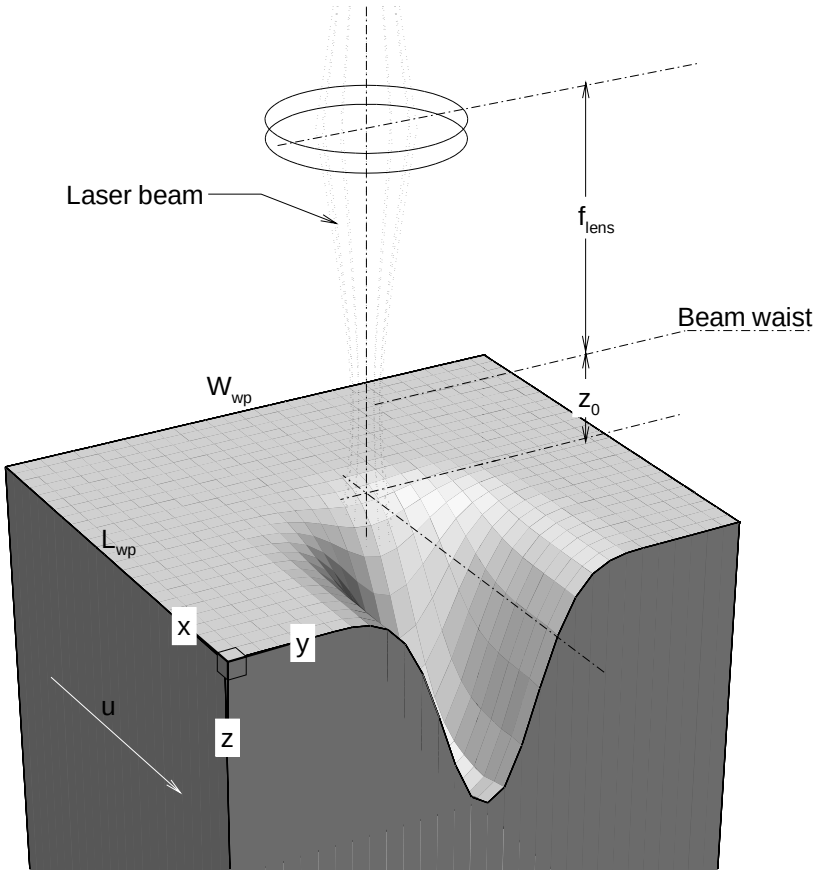

Figure 1: Laser ablation setup and coordinate system.

laser beam that moves with constant velocity u into the positive $\overline{x}$-direction (see Fig. 1) may be expressed in terms of temperature T as:

$$\rho c \frac{\partial T}{\partial \overline{t}} = \boldsymbol{\nabla} \cdot (k \boldsymbol{\nabla} T), \tag{1}$$

subject to the boundary conditions,

$$\overline{y} = 0,\ \overline{y} = W_{wp}: \quad \frac{\partial T}{\partial \overline{y}} = 0, \tag{2a}$$

$$\overline{x} = 0,\ \overline{x} = L_{wp}: \quad \frac{\partial T}{\partial \overline{x}} = 0, \tag{2b}$$

$$\overline{z} \rightarrow +\infty: \quad T = T_{\infty}, \tag{2c}$$

$$\overline{z} = \overline{s}(\overline{x}, \overline{y}): \quad \alpha \mathbf{F} \cdot \hat{\mathbf{n}} = -\hat{\mathbf{n}} \cdot (k \boldsymbol{\nabla} T) + v_n \rho \Delta h_{re} \tag{2d}$$

and an appropriate initial condition, such as

$$\overline{t} = 0: \quad T(\overline{x}, \overline{y}, \overline{z}, 0) = T_{\infty},$$
$$\overline{s}(\overline{x}, \overline{y}, 0) = \overline{s}_0(\overline{x}, \overline{y}), \tag{2e}$$

where v_n is the surface recession velocity (and some quantities have been barred to distinguish the present dimensional quatities from the nondimensional ones introduced below).

Boundary condition (2*d*) states that the irradiation absorbed at the surface is used up by conduction losses into the solid and by evaporation, if present (if no evaporation takes place, *i.e.*, during warm-up, cool-down and in regions too far away sideways from the laser beam, the surface recession velocity vanishes, *i.e.*, $v_n = 0$). The energy intensity distribution, **F**, for a focussed Gaussian laser beam having a waist w_0 at the focal plane z_0, moving with constant velocity u into the positive $\overline{x}$ direction, has been given by Kogelnik and Li [20] and is described in detail in Refs. [14, 16, 19].

Boundary conditions (2) are sufficient to solve equation (1) for the temperature if the groove shape s is already established ($v_n = 0$) or if v_n is otherwise known. As in Modest [19], we will assume in this paper that the ablation and/or decomposition of the solid material is governed by a simple reaction equation of the Arrhenius type, *i.e.*, the rate of mass loss per unit area is described by

$$\dot{m}'' = \rho v_n = \rho C_1 e^{-E/\overline{R}T}, \tag{3}$$

where E is the decomposition energy, $\overline{R}$ is the universal gas constant, and C_1 is a preexponential factor that depends on the nature of the ablation process (see, *e.g.*, Wei and Ho [21] for simple evaporation).

Before attempting a numerical solution, the governing equations and boundary conditions are non-dimensionalized using the 86%-beam radius at the focal point, w_0:

$$x = \overline{x}/w_0; \quad y = \overline{y}/w_0; \quad z = \overline{z}/w_0; \quad s = \overline{s}/w_0; \quad \theta = \frac{T - T_\infty}{T_{re} - T_\infty}. \tag{4}$$

This leads to three basic non-dimensional parameters governing the laser/material interaction:

$$U = \frac{\rho c_{re} u w_0}{k_{re}}; \quad N_k = \frac{k_{re}(T_{re} - T_\infty)}{F_0 w_0}; \quad \text{Ste} = \frac{\Delta h_{re}}{c_{re}(T_{re} - T_\infty)} \tag{5}$$

(More detail, in particular for variable properties, is given in [19]). Physically, N_k approximates the ratio of conduction losses, for a surface normal to irradiation, and the absorbed laser flux; Ste is a Stefan number that compares ablation energy with sensible heat, and U relates the laser scanning speed to that of thermal diffusion into the medium.

The present set of equations is similar to the one used previously except that the boundary and initial conditions have been modified: in [19] half of a symmetric groove carved into a flat, infinitely large piece of material was calculated; here we consider a workpiece of finite length and width (to allow the determination of laser entry and exit effects) and variable surface topography (*e.g.*, the output geometry from one grooving operation may be used as input to another calculation to study the groove resulting from multiple, partially-overlapping laser scans).

Boundary-fitted coordinates are employed in the numerical solution, *i.e.*, the physical domain (x, y, z), is transformed to a uniformly spaced rectangular coordinate region (ξ, η, ζ) (see Refs. [14, 16, 19] for details). However, previous publications were limited to single, (half-)grooves in an infinite medium, which could be treated with a relatively simple three-dimensional grid system. To calculate laser shaping events such as grooving with effects of pulsing, turn on, turn off, entrance and exit effects, as well as forming of several parallel, partially-overlapped grooves, a "workpiece" (for the calculations) must be constructed, which includes all parts that are ever (during any of the individual operations) influenced by the laser. To get an accurate description

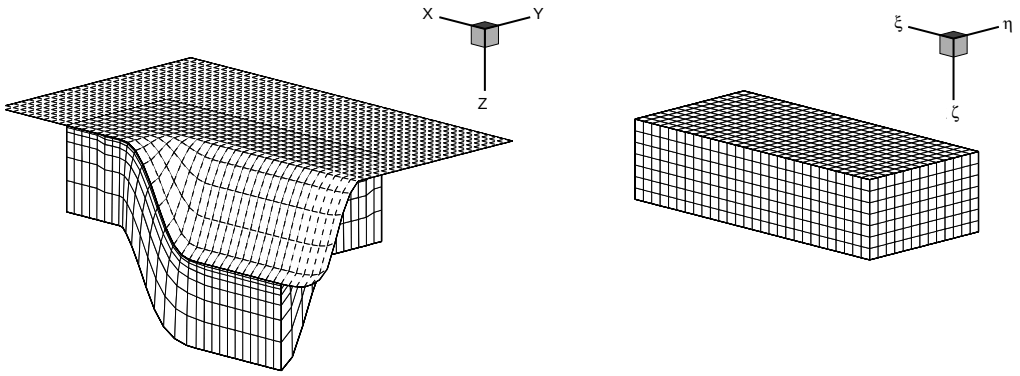

Figure 2: Physical and computational grid systems.

of the overall process, the topography of this workpiece must be described through a large two-dimensional network. Expanding this nodal network to three dimensions to allow temperature and shaping calculations is not possible (requiring hundreds of megabytes of computer storage), nor is it necessary. Instead, a two-layered grid system was constructed: a two-dimensional one consisting of $NS_\xi \times NS_\eta$ nodal points to describe the topography of the laser-irradiated surface of the workpiece, and a second, three-dimensional system consisting of $N_\xi \times N_\eta \times N_\zeta$ nodal points to describe that part of the workpiece that is – at any given time – affected by the laser (*i.e.*, whose temperature is raised). This region is bounded by the irradiated surface ($\zeta = 1$), and another surface ($\zeta = N_\zeta$), "far" away into the body not heated by the laser. Grid points of the three-dimensional system at the irradiated surface ($\zeta = 1$) are identical to a subset of the nodal set describing the surface topography. As the laser moves across the surface different parts of the workpiece become heated by the laser beam. Thus, nodes are continously added ahead of the laser beam and dropped in its rear. It is desirable to maintain uniform nodal spacing of $\Delta\xi = \Delta\eta = \Delta\zeta = 1$ between the nodal points, which simplifies difference representation in the computational space. In Fig. 2 the three-dimensional computational domain (ξ, η, ζ), which is a rectangular parallelepiped, is shown alongside the physical domain which shows the two-tiered nodal system: surface topography nodes are shown by dashed lines, and volume coordinates (corresponding to the parallelepiped of the computional domain) are shown in solid.

A number of considerations are important for the construction of the computational nodal system:

1. The nodal system must be smoothly distributed across the computational domain; nodes may not be spaced apart too much wherever substantial temperature gradients are expected.
2. The grid system needs to be self-adaptive, automatically deforming itself as the laser removes and shapes material.
3. Because of the rapid recession and deformation of the computational domain the nodal network needs to be recalculated during each time step; therefore, the nodal network construction must be very simple to allow rapid recalculation.

These above considerations make the construction of a three-dimensional grid system a formidable problem! Thankfully, the problem is somewhat simplified by the fact that the heat-affected zone is usually only a thin surface layer, ranging in thickness from 1 to 2 laser radii for CW laser operation to as little as 0.1 radii and less for pulsed operation. Thus, the problem may be broken up into two

parts: (i) generation of the nodal network on the top (irradiated surface), and (ii) calculation of internal nodes. Computational efficiency dictates that all grid generation needs to be done using simple algebraic interpolation functions.

Surface nodes The overall extent of the workpiece is assumed to be rectangular. A simple hole drilled into the workpiece would produce a deep, circular indentation in a rectangular body. All two-dimensional methods to produce a "good" network on such a system as described by Thompson et al. [22] were tried and failed, since a) they have difficulty accomodating a circular shape within a rectangular frame, and b) they have great difficulty placing regular nodes on the sharp apex of a deep hole. On the other hand, for the vast majority of problems it is quite acceptable to use constant spacing in the x- and y-directions (Δx = const, Δy = const): grid spacing tends to get large only on very steep surfaces; these steep surfaces, however, tend to be almost isothermal (since ablation is taking place on their surface) without substantial conduction along them, or they are far away from the laser-interaction zone (*i.e.*, they are unimportant). Exceptions to this rule are cases with strong internal reflections and/or a strongly diverging laser beam focused inside the workpiece: in both cases the sidewalls may become **very** steep or even fold back (*i.e.*, the width of the groove inside may be larger than near the surface). We will limit ourselves here to constant spacing in the x- and y-directions.

Internal Nodes Once the surface nodes have been established, the internal grid points for each surface node need to be generated. Lines of (ξ = const, η = const) need to move smoothly from the surface (ζ = 1) to a point "far" inside the material ($\zeta = N_\zeta$); the various lines may not interfere with one another, indeed, they should stay as far apart as possible everywhere to minimize numerical instability. Near the surface (where the largest temperature gradients are) the lines need to be perpendicular to the surface (to minimize truncation error [22]). Therefore, the internal nodal system is designed such that the local unit tangent to a (ξ = const, η = const) line is equal to the surface normal near the irradiated surface and blends gradually to the desired gridline direction at a"far-inside" point $\zeta = N_\zeta$ (see [19] for details). The non-dimensionalized and transformed version of (1) is finite-differenced and solved using a semi-implicit algorithm. In this scheme θ_ζ and $\theta_{\zeta\zeta}$ (*i.e.*, derivatives normal to the thin heat-affected layer) are finite-differenced implicitly as is the non-linear ablation condition. All other derivatives are finite-differenced explicitly without loss of stability, as explained in Ref. [19].

SAMPLE RESULTS AND COMPARISON WITH EXPERIMENTS

The present computer code was executed for a number of input parameters, to study the effects of a laser scanning across the edges of a workpiece, either entering or exiting the material, as well as the behavior of multiple, parallel, partially-overlapping grooves. In order to compare the theoretical results with experimental grooves on graphite obtained with a CW CO_2 laser, all calculations were done using the thermophysical properties of graphite, as obtained from the JANAF tables [23] (heat of removal Δh_{re}) and the Purdue series on thermophysical properties [24–27] (absorptance α, thermal conductivity k_{re}, thermal diffusivity $\alpha_{H,re} = k_{re}/\rho c_{re}$), all evaluated at the estimated ablation temperature of T_{re} = 4000 K.

Thermophysical Properties High temperature values for the thermal diffusivity of graphite range between $\alpha_H \simeq 0.002$ and 0.06 cm^2/s, with most data near 3000 K being around $\alpha_H \simeq$ 0.03 cm^2/s [27]. Similarly, data for thermal conducitivity range from k = 0.1 to 0.4 W/cmK [25], while data for specific heat are somewhat more consistent at $c \simeq$ 2.0 to 3.2 J/gK [24]; even the

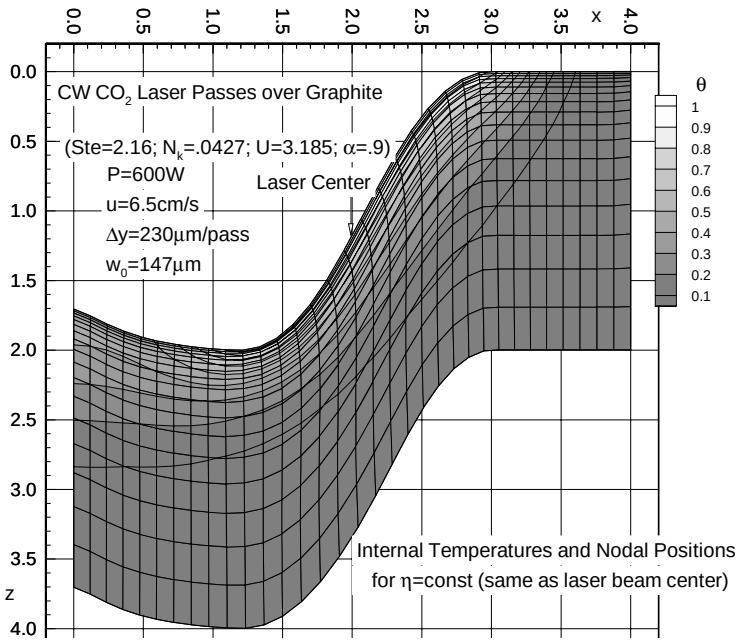

Figure 3: Groove development along centerline.

density of different types of graphite can vary considerably between about ρ = 1.5 and 2.5 g/cm^3. For comparison with theoretical calculations a self-consistent set of thermophysical properties was chosen as k_{re} = 0.15 W/cmK, ρ_{re} = 2.0 g/cm^3, c_{re} = 2.5 J/gK which leads to $\alpha_{H,re}$ = 0.03 cm^2/s. Reported spectral absorptances also vary widely, between $\alpha \simeq 0.15$ and 0.95 [26]; however, most graphites tend to be highly absorptive across the infrared, and an α_{re} = 0.9 was chosen for the comparison. Finally, the heat of removal was calculated from enthalpy values given in the JANAF tables [23]: subtracting the enthalpy of solid graphite from those of gaseous carbon leads to $\Delta h \simeq 20$ kJ/g (graphite decomposes into pure C_3), $\Delta h \simeq 34$ kJ/g (pure C_2) and $\Delta h \simeq 59$ kJ/g (pure C). Since decomposition products are expected to be almost pure C_3 [23], a Δh_{re} = 20 kJ/g was chosen for all calculations.

All calculations were performed on a "workpiece" 4 beam radii long and 6 beam radii wide. Keeping the workpiece as small as possible (without compromising accuracy) minimizes CPU time and, particularly, computer memory requirements, and facilitates graphical presentation of results, showing greater detail. A workpiece of length $L_{wp} = 4w_0$ is sufficient to display entry effects, to attain a small fully-developed groove section, and to show the laser exit effects. A width of $W_{wp} = 6w_0$ (and using symmetry at y = 0 by insulating that surface), on the other hand, is wide enough to study the shaping of three parallel, offset grooves.

Figure 3 shows a typical x-z-plane cut through the workpiece (at y = const = 3.13 = the value at which the center of the laser beam pans across the material). It simulates the case of a CW CO_2 laser beam scanning over a piece of graphite with a power of 600 W and a speed of 6.5 cm/s. The beam is focussed by a 5″ (12.7 cm) plano-convex lens, has a spotsize of w_0 = 147 μm and a beam quality factor M^2 = 2.7 (which affects the spreading of the beam beyond the focal point). The figure shows the development of the center of the groove as the laser scans across the surface, entering it at x = 0 and presently having reached the position x = 2.0. The figure also shows the

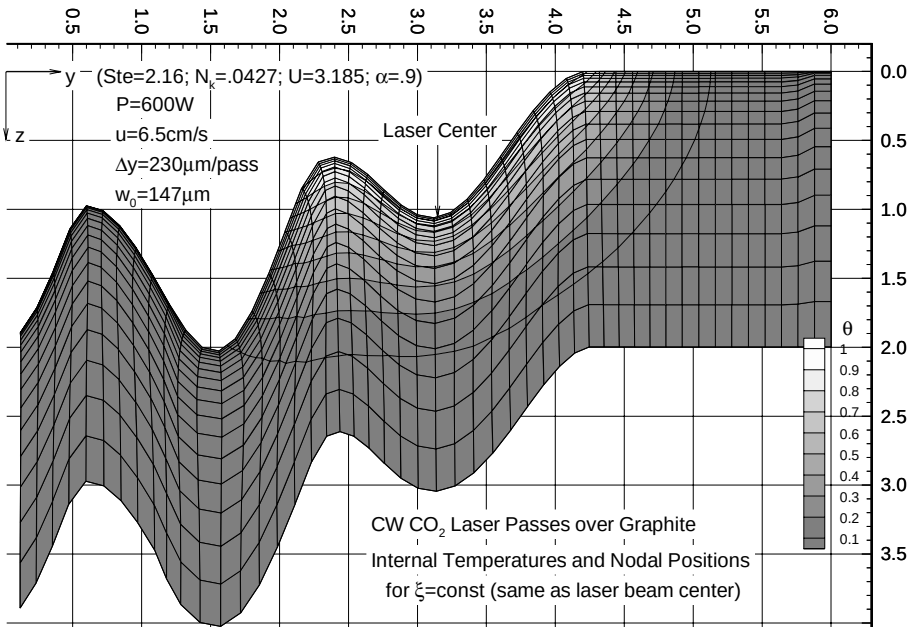

Figure 4: Groove cross section at the center of laser beam.

nodal system as it is being generated by the code: ζ-lines start normal to the groove surface and then gradually turn to the vertical, until they reach the end of the heat-affected layer (here, for the CW case, conservatively taken as $2\,w_o$ thick). Note how close to the surface the first few nodes are due to the severe temperature gradients. Also shown in the figure are internal isotherms, indicating that strong ablation takes place over a length of $\simeq 2\,w_o$ (one radius ahead of the laser center, and one behind), that the preheating zone in front of the laser is rather short ($\simeq 0.5\,w_o$), while cooling down behind the laser is very gradual. The isotherms also show that the heat-affected zone is thinnest where ablation is strongest: the ablation front is trying to catch up with the diffusion front.

Figure 4 shows a y-z-plane cut through the workpiece (at x = 2.0 = const = the preset x-position of the center of the laser beam) for the identical case and time as Fig. 3. At the time shown the laser is in the middle of its third pass across the workpiece. The first full pass was done at y = 0. Note that a part of the first groove is truncated in Fig. 4: the calculations are presently considering the third pass, part of the first groove is too far away sideways from the present laser position to affect the results, and the 3-D internal nodal system is cut off accordingly. After completion of the first pass (and sufficient cool-down) the laser is returned to a position $x \ll 0$ and moved sideways to the position y = 230 μm/147 μm = 1.56. Then the laser scans across the surface again. Note that the second groove is deeper than the first, since the first pass removed already some material in the path of the second pass (this gives rise to an unsymmetric groove cross section, as will be seen more clearly later). Careful scrutiny of the figure also reveals that the first inside nodes are closer to surface near the laser center than further to the sides, due to the steeper temperature gradients there.

Finally, Fig. 5 shows a three-dimensional surface view of the case described in Figs. 3 and 4: the laser enters the material from the right, scans across the workpiece and leaves it on the left. The figure shows, qualitatively, the entrance and exit effects. The grooves tend to be less deep where

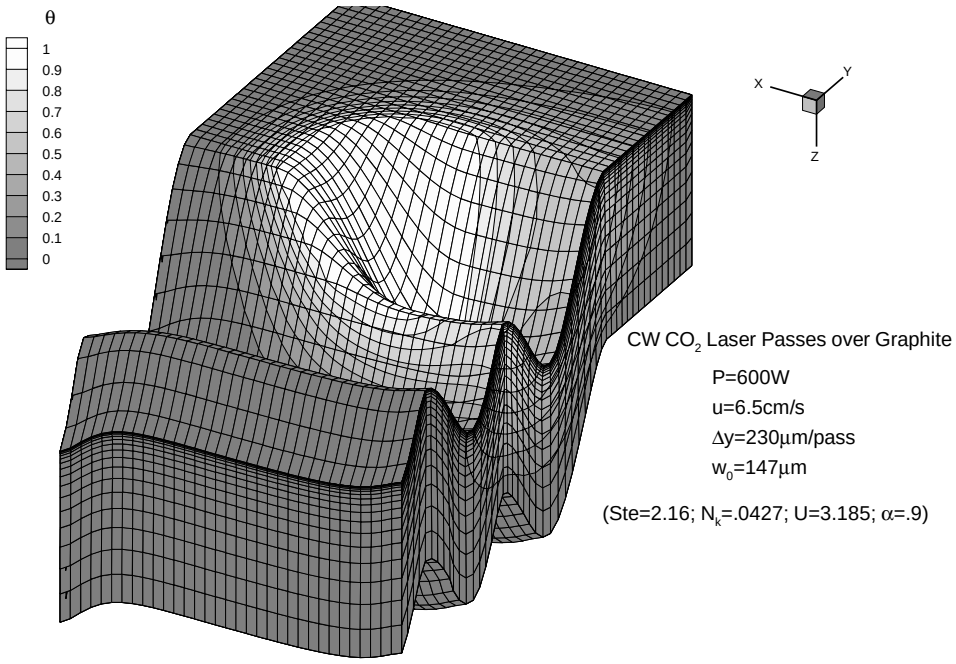

Figure 5: Three-dimensional view of overlapping groove development and surface temperatures (CW laser).

the laser enters the material (as compared to the fully-developed groove depth further inside the material). This is apparently due to the fact that no forward diffusion takes place just before entry, and the material must be preheated locally. For the same reason the opposite effect is observed at the laser exit: no forward diffusion takes place so that at the exit additional energy is trapped resulting in a deeper groove.

These entry and exit effects are shown in Fig. 6 for two cases: (a) a 600 W CW CO_2 laser scanning at 6.5 cm/s (*i.e.*, the case of Figs. 3 through 5), and (b) a 800 W CW laser scanning at 8 cm/s. For comparison, single grooves were cut in graphite for identical lasing conditions: all samples (square graphite plates 50 mm $\times$ 50 mm $\times$ 5 mm) where scribed with a *Coherent MS51* CO_2 laser focused with a 5″ plano-convex ZnSe lens. Argon at a flowrate of 50 ft^3/hr was used as gas assist to minimize redeposition and oxidation (burning). In general, considerable amounts of velvety, black soot deposits were observed in and all around the grooves, which was blown away with compressed shop air before further evaluation. At the focal point the laser intensity was approximately Gaussian with a spot size of $w_0 \simeq 147\,\mu$m and a beam quality factor of $M^2 \simeq 2.7$. To measure groove depths along centerlines the specimens were first cut with a diamond saw near the center of the groove. The graphite was polished with a motorized wheel (1200 grit) parallel to the centerline accompanied by frequent checking under the microscope until the centerline was reached. Groove depths were measured with two perpendicular digital micrometer-driven stages that were attached to a measuring microscope. Because only a single entry and exit were measured for each case, because of surface roughness and because of the inherent inaccuracy of the measuring technique, the results are somewhat qualitative. Comparison with theory shows that the model predicts the trends very well: lesser groove depth at entry, and a deepening at the exit. However, experiment seems to suggest much stronger effects than predicted by theory. In fact,

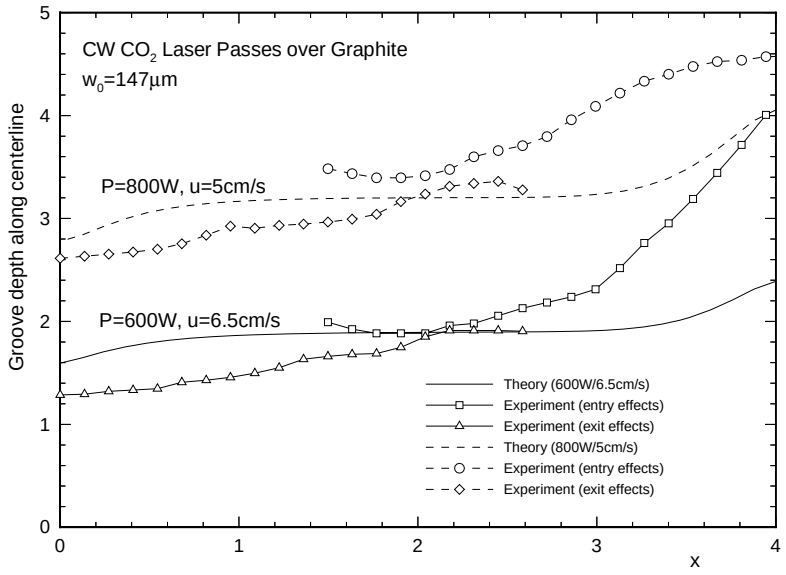

Figure 6: Entrance and exit effects on groove development along centerline.

agreement is better than Fig. 6 suggests, since exit cross sections were consistently triangular in shape with a sharp apex at the centerline, exaggerating the exit effects there. The reason behind these stronger exit effects near the centerline remains presently unknown. Possibly, the hot graphite burns after the laser (and the argon jet) exits the material (since ambient oxygen can reach the exit plane much better than internal parts of the groove). Also, microscope observation of the 600 W/6.5 cm/s-specimen suggests that beyond $x > 3$ a small piece may have broken out.

For comparison, Fig. 7 shows a similar view of graphite machined with a Q-switched laser. To stay within realistic limits a total, nondimensional pulse period of 0.14 was chosen (corresponding to a repetition rate of approximately 1kHz), and a square pulse shape was used of duration $0.14/2000 = 7 \times 10^{-5}$ (approximately 500ns). Note that the heat-affected layer is very thin ($< 0.025 w_0$), so that calculations are only carried out to a depth of $0.06 w_0$ below the surface. The temperature drop-off zone to the sides is also much thinner resulting in a larger ablation zone. For this situation conduction losses are below 5% and, therefore, entry and exit effects are hardly noticeable (except for a small dip at the netry). Note also that the bottom of the grooves are rather smooth despite the fact that the laser moves by the rather large distance of $0.14 \times 3.185 = 0.446 w_0$ between any two pulses.

Finally, Fig. 8 shows the cross sections of fully-developed overlapped grooves for the 600 W-6.5 cm/s case and compares them with experimental data. In the experiments six passes were made across the graphite sample using identical laser and workstation parameters. Between each pass the sample was allowed to cool for 2 minutes, and the y-stage (perpendicular to the laser scan direction) was moved by 230 μm. Two profilometers were available to determine the cross sections of the resulting grooves: an optical, laser-based device for maximum depths of 250 μm (*Focodyn* by *Perthen*) and a mechanical device for depths up to 750 μm (*Perthometer* by *Perthen*). Unfortunately, the optical device failed, probably because of the steep walls in the grooves. The mechanical device was able to measure the central three grooves, failing near the sides due to its relatively blunt tip. Groove cross sections were measured as follows: five passes across the six grooves were made in close proximity to each other (within a range of $\sim$ 2 mm), and the

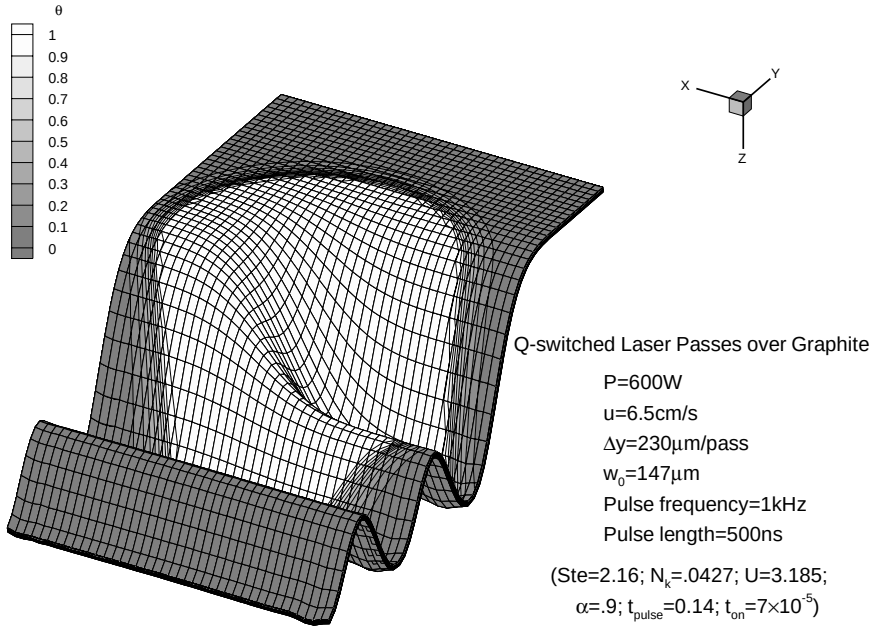

Figure 7: Three-dimensional view of overlapping groove development and surface temperatures (Q-switched laser).

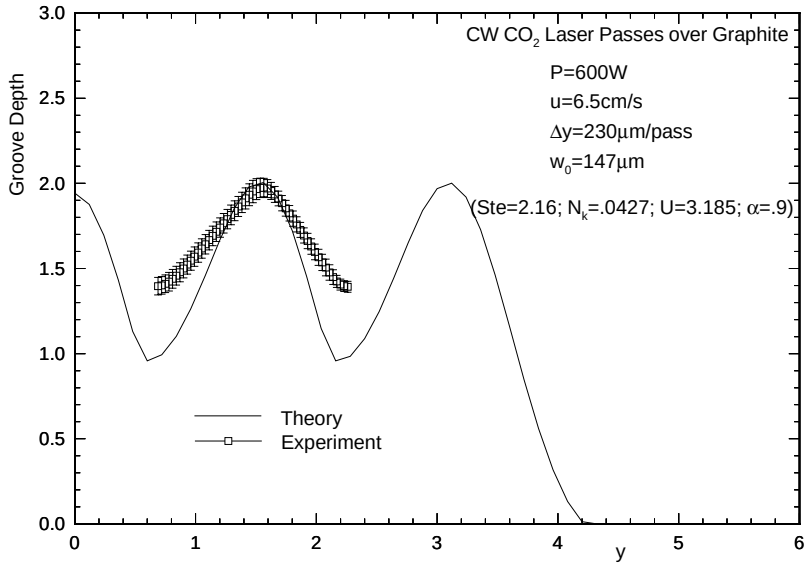

Figure 8: Groove cross sections for multiple, parallel, partially-overlapping laser passes.

results were stored in a microcomputer. The *Perthometer* was then turned off and the sample removed. The measurements were then repeated at a later time at a different location of the 50 mm long grooves. Thus a total of 30 tip-to-tip groove cross section data sets were obtained: 2×5 *Perthometer* passes each providing data for the 3 central grooves. The results of the average groove cross section are displayed in Fig. 8 together with their standard deviation ($\pm 1\sigma$), along with theoretical predictions (for three laser passes, *i.e.*, only the central one is "fully developed"). Considering the uncertainty of thermophysical property and laser data as well as laser output instabilities, the agreement between theory and experiment is surprisingly good: theory predicts the maximum groove depth correctly, and shows a similarly asymmetric profile as the experiment does (grooves are deeper on the sides where a small amount has already been removed during the previous pass). However, theory predicts a much larger ridge between grooves. This may be due to a number of factors:

1. The hot ridges burn after the laser has passed, resulting in a porous structure, which gets blown out during cleaning (this is supported by microscope pictures of several runs, which showed irregular remnants on the ridges).
2. The mechanical force exerted by the profilometer tip may flatten the ridge between grooves (however, since the standard deviation shown is Fig. 8 is rather small, this flattening would have to be rather repeatable).
3. The actual beam radius and/or beam quality factor may be somewhat larger than assumed in the calculation; this would imply a smaller relative step between grooves, resulting in flatter ridges.

SUMMARY AND CONCLUSIONS

Our three-dimensional conduction model has been extended to allow the calculation of real laser shaping processes, such as laser entry and exit effects, shapes resulting from multiple, parallel, partially-overlapping laser passes, *etc*. The model allows the very efficient calculation of shapes and temperature fields for lasers operating in CW or pulsed mode (with pulse times measured in ms, or very short pulses measured in ns), applied to materials with constant or temperature-dependent thermophysical properties. Comparison with experimental data obtained with a CW CO_2 laser on graphite shows good qualitative agreement. Even quantitative agreement may be considered very good, if one takes into account how poorly material properties at high temperatures are known, and how variable laser grooves tend to be (due to laser power instabilities, work station inaccuracy, and material inhomogeneity).

Acknowledgment

This work was carried out while the author was on sabbatical leave at the Institut für Strahlwerkzeuge (IFSW), University of Stuttgart, Germany. Their partial support and the support of the SEW-EURODRIVE Foundation are gratefully acknowledged.

References

1. F. W. Dabby and U.-C. Paek, High-Intensity Laser-Induced Vaporization and Explosion of Solid Material, *I.E.E.E. J. Quantum Electron.*, **QE-8**, 106–111 (1972).

2. R. E. Wagner, Laser Drilling Mechanics, *J. Appl. Phys.*, **45**, 4631–4637 (1974).
3. D. Schuöecker and W. Abel, Material Removal Mechanism of Laser Cutting, In *Proceedings of the SPIE*, (1983).
4. D. Petring, P. Abels, and E. Beyer, Werkstoffbearbeitung mit Laserstrahlung, *Feinwerktechnik and Messtechnik*, **96**, 364–372 (1988).
5. C. L. Chan and J. Mazumder, One-Dimensional Steady-State Model for Damage by Vaporization and Liquid Expulsion Due to Laser-Material Interaction, *J. Appl. Phys.*, **62**(11), 4579–4586 (1987).
6. M. F. Modest and H. Abakians, Heat Conduction in a Moving Semi-Infinite Solid Subjected to Pulsed Laser Irradiation, *J. Heat Transfer*, **108**, 597–601 (1986).
7. M. F. Modest and H. Abakians, Evaporative Cutting of a Semi-Infinite Body With a Moving CW Laser, *J. Heat Transfer*, **108**, 602–607 (1986).
8. H. Abakians and M. F. Modest, Evaporative Cutting of a Semi-Transparent Body with a Moving CW Laser, *J. Heat Transfer*, **110**, 924–930 (1988).
9. S. Ramanathan and M. F. Modest, Effect of Variable Properties on Evaporative Cutting with a Moving CW Laser, In *Heat Transfer in Space Systems*, Vol. HTD–135, ASME, (1990).
10. S. Ramanathan and M. F. Modest, Single and Multiple Pass Cutting of Ceramics With a Moving CW Laser, In *Proceedings of the XXII ICHMT Intl. Symposium on Manufacturing and Materials Processing*, Dubrovnik, Yugoslavia, (1990).
11. S. Ramanathan and M. F. Modest, CW Laser Drilling of Composite Ceramics, In *Proceedings of ICALEO '91, Laser Materials Processing*, Vol. 74, San Jose, CA, 305–326 (1992).
12. S. Ramanathan and M. F. Modest, CW Laser Cutting of Composite Ceramics, In *Laser Advanced Materials Processing – LAMP '92*, Vol. 2, Nagaoka, Japan, 625–632 (1992).
13. S. Roy and M. F. Modest, Three-Dimensional Conduction Effects During Evaporative Scribing with a CW Laser, *J. Thermoph. Heat Transfer*, **4**(2), 199–203 (1990).
14. S. Roy and M. F. Modest, Evaporative Cutting with a Moving CW Laser — Part I: Effects of Three-Dimensional Conduction and Variable Properties, *Int. J. Heat Mass Transfer*, **36**(14), 3515–3528 (1993).
15. S. Y. Bang and M. F. Modest, Multiple Reflection Effects on Evaporative Cutting with a Moving CW Laser, *J. Heat Transfer*, **113**(3), 663–669 (1991).
16. S. Y. Bang, S. Roy, and M. F. Modest, CW Laser Machining of Hard Ceramics — Part II: Effects of Multiple Reflections, *Int. J. Heat Mass Transfer*, **36**(14), 3529–3540 (1993).
17. S. Y. Bang and M. F. Modest, Evaporative Scribing with a Moving CW Laser - Effects of Multiple Reflections and Beam Polarization, In *Proceedings of ICALEO '91, Laser Materials Processing*, Vol. 74, San Jose, CA, 288–304 (1992).
18. G. Chryssolouris, *Laser Machining: Theory and Practice*, Springer Verlag, New York, NY, 1st ed., (1991).
19. M. F. Modest, Three-Dimensional, Transient Model for Laser Machining of Ablating Materials, *Int. J. Heat Mass Transfer*, (1994), Submitted for publication.
20. H. Kogelnik and T. Li, Laser Beams and Resonators, *Appl. Opt.*, **5**(10), 1550–1565 (1956).

21. P. S. Wei and J. Y. Ho, Energy Considerations in High-Energy Beam Drilling, *Int. J. Heat Mass Transfer*, **33**(10), 2207–2218 (1990).
22. J. F. Thompson, Z. U. A. Warsi, and C. W. Mastin, *Numerical Grid Generation, Foundations and Applications*, North-Holland, New York, (1985).
23. Jr. M. W. Chase, C. A. Davies, Jr. J. R. Downey, D. J. Frurip, R. A. McDonald, and A. N. Syverud, eds., *JANAF Thermochemical Tables*, National Bureau of Standards, Washington, DC, (1985).
24. Y. S. Touloukian and E. H. Buyco, eds., *Specific Heat: Nonmetallic Solids*, Vol. 5 of *Thermophysical Properties of Matter*, Plenum Press, New York, (1970).
25. Y. S. Touloukian, R. W. Powell, C. Y. Ho, and P. G. Klemens, eds., *Thermal Conductivity*, Vol. 2 of *Thermophysical Properties of Matter*, Plenum Press, New York, (1970).
26. Y. S. Touloukian and D. P. DeWitt, eds., *Thermal Radiative Properties: Nonmetallic Solids*, Vol. 8 of *Thermophysical Properties of Matter*, Plenum Press, New York, (1972).
27. Y. S. Touloukian, R. W. Powell, C. Y. Ho, and M. C. Nicolaou, eds., *Thermal Diffusivity*, Vol. 10 of *Thermophysical Properties of Matter*, Plenum Press, New York, (1973).